JOURNAL OF SOLID STATE CHEMISTRY 18, 27–37 (1976)

Crystal Chemistry of MSeO$_3$ and MTeO$_3$ (M = Mg, Mn, Co, Ni, Cu, and Zn)

KAY KOHN,* KATSUHIKO INOUE,†‡ OSAMU HORIE,*§ AND SYUN-ITI AKIMOTO†**

* *Department of Physics, School of Science and Engineering, Waseda University, Shinjuku-ku, Tokyo 160, Japan, and*
† *Institute for Solid State Physics, The University of Tokyo, Minato-ku, Tokyo 160 Japan*

Received December 17, 1975

New selenites and tellurites $MgSeO_3$, $MnSeO_3$, $CoSeO_3$, $NiSeO_3$, $CuSeO_3$, $MnTeO_3$, $CoTeO_3$, and $NiTeO_3$ were synthesized under high pressures and temperatures. All the compounds are isomorphous and their crystal system is orthorhombic. Structure analyses were carried out for all the selenites and $CoTeO_3$. The structure is described as a salt of M^{2+} and SeO_3^{2-} or TeO_3^{2-} ions or as a distorted perovskite. In these compounds an Se or Te atom is closely linked to three oxygen atoms to form a flattened trigonal pyramid. The features of this coordination are discussed. At low temperature, magnetic order appears in all the compounds containing iron group ions, among which $CuSeO_3$ is a ferromagnet with the Curie temperature of 26°K.

Introduction

Ions with a nonbonded s-electron pair such as Tl^+, Ge^{2+}, Sn^{2+}, Pb^{2+}, As^{3+}, Sb^{3+}, Bi^{3+}, Se^{4+}, Te^{4+}, etc., play a peculiar role in crystal chemistry because of their high polarizability and strong preference to unusual stereochemistry. They are usually found in an asymmetric environment in crystals. In other words, such an ion A has a tendency to form a coordination polyhedron AX_n lacking a center of symmetry. This is interpreted as a result of an off-center displacement of A in a coordination polyhedron due to the mixing of s and p orbitals (*1*). In another interpretation it is a result of the formation of hybrid orbitals, one of which is occupied by nonbonded s-electrons (*2*). For instance, we will take an AX_3 group with a trigonal pyramidal shape, which is the most commonly found. In the first view, it is obtained by the displacement of the central atom A of a regular octahedron AX_6 along the three fold axis, while in the latter it is considered as a tetrahedral AX_3E group, where one of the orbitals is occupied by a nonbonded pair E.

Although not a few structural data are present about the compounds containing these ions, systematic studies of their crystal chemistry are scarce. In addition, crystal structure with such an off-center distortion is possibly accompanied with various interesting physical properties. Possible relations to ferroelectricity (*1*) and nonlinear optical properties (*3*) have been discussed. New compounds with interesting structural and physical properties are therefore expected to be found in such crystal chemical studies.

‡ On leave from Asada Fundamental Research Laboratory, Kobe Steel Ltd., Nada-ku, Kobe 657, Japan.

§ Present address: The Research Institute for Iron, Steel and Other Metals, Tohoku University, Sendai 980, Japan.

** Correspondence should be addressed to Syun-iti Akimoto, Institute for Solid State Physics, The University of Tokyo, Minato-ku, Tokyo 106, Japan.

Copyright © 1976 by Academic Press, Inc.
All rights of reproduction in any form reserved.
Printed in Great Britain

The double oxides of the ions with a non-bonded *s*-electron pair and an iron group transition metal ion are of particular interest in view of possible interactions between dielectric and magnetic properties. In this connection, many works have been reported about the oxides containing Pb^{2+} and Bi^{3+} ions (*4*). Little has been known, however, about the other compounds. Recently, we succeeded in the high-pressure synthesis of several new compounds of the type MAO_3, where M is Mg, Mn, Co, Ni, Cu, or Zn and A is Se or Te (*5*, *6*). This paper reports the synthesis, stability fields, crystal structure, and magnetic properties of these compounds. The structure is discussed from two different standpoints, that is, it is at first described as a salt of M^{2+} and AO_3^{2-} ions, and then as a double oxide of M^{2+} and A^{4+} ions. Discussions about the coordination of oxygen about Se or Te and the distortion and the tilt of an MO_6 octahedron are given.

Experimental Details and Results

Synthesis

All the compounds were synthesized by direct solid-state reaction under high pressures and temperatures. Equilmolar amounts of a monooxide MO (M = Mg, Mn, Co, Ni, Cu, or Zn) and SeO_2 or TeO_2 were intimately mixed and subjected to high pressures between 15 and 70 kbar in a tetrahedral-anvil type of high-pressure apparatus. Reaction temperatures were between 50 and 1000°C. Lengths of run time were varied from 20 to 60 min, depending on the reaction temperature. Samples were quenched in the conventional method under working pressure. In several runs, the mixture was prefired at 700°C in a sealed-off gold tube prior to the high-pressure reactions. No remarkable differences were discerned between the results of the runs with and without this prefiring. The quenched materials were well-crystallized powder with a specific color shown in the last row of Table I.

Stability Fields and Lattice Parameters

Quenched-products were examined by X-ray diffraction with a diffractometer. The synthesis diagrams determined from the X-ray data are shown in Fig. 1. New compounds were obtained in the pressure range higher than certain boundaries, which are almost independent of temperature. All the observed diffraction lines of these high-pressure phases were well indexed on an orthorhombic cell. $CuSeO_3$ was found to have two different forms in a lower pressure range. The products from the mixtures of MO (M = Mn, Co, or Ni) and TeO_2 in lower pressure were two-phase mixtures of rocksalt type MO and monoclinic $M_2Te_3O_8$ (*7–9*). As for the other compounds, low-pressure products could not be identified.

The final lattice parameters of the high-pressure phase of MAO_3 compounds were obtained by accurate measurements of 2θ values for all the observed reflections between 25° and 130° and by least-squares refinements. Fe$K\alpha_1$ radiation was used throughout. The results are given in Table I.

Intensity Measurements

Structure analyses were carried out for all the synthesized selenites $MgSeO_3$, $MnSeO_3$, $CoSeO_3$, $NiSeO_3$, $CuSeO_3$, and $ZnSeO_3$ and

TABLE I

COLOR AND FINAL LATTICE PARAMETERS OF MAO_3

	$MgSeO_3$	$MnSeO_3$	$CoSeO_3$	$NiSeO_3$	$CuSeO_3$	$ZnSeO_3$	$MnTeO_3$	$CoTeO_3$	$NiTeO_3$
a (Å)	5.9246 (5)	6.0945 (4)	5.9297 (4)	5.8803 (3)	5.9652 (10)	5.9231 (4)	6.1443 (4)	6.0169 (3)	5.9564 (3)
b (Å)	7.6663 (8)	7.8656 (8)	7.5954 (4)	7.5235 (4)	7.3265 (13)	7.6652 (8)	7.7866 (7)	7.5147 (5)	7.4986 (4)
c (Å)	5.0059 (5)	5.1460 (4)	5.0293 (2)	4.9394 (2)	5.2828 (8)	5.0400 (6)	5.4408 (4)	5.3266 (3)	5.2128 (2)
Color	White	Light sepia	Violet	Yellowish green	Green	White	Light sepia	Violet	Yellowish green

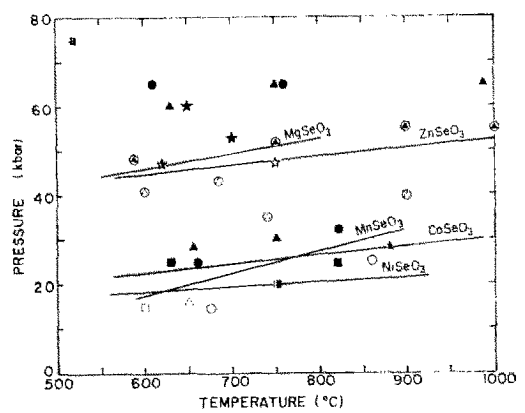

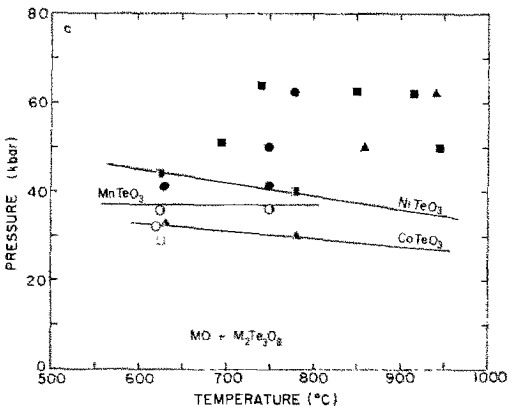

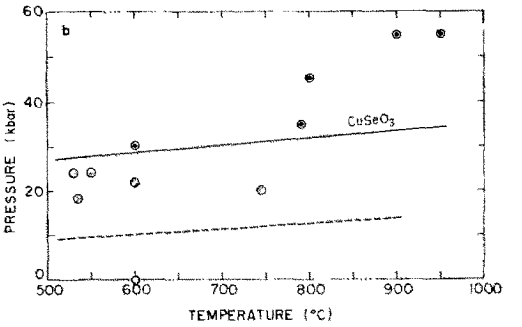

FIG. 1. (a) Synthesis diagram of $MgSeO_3$, $MnSeO_3$, $CoSeO_3$, $NiSeO_3$, and $ZnSeO_3$. (b) Synthesis diagram of $CuSeO_3$. (c) Synthesis diagram of $MnTeO_3$, $CoTeO_3$, and $NiTeO_3$. In these diagrams, solid circles (Mn), triangles (Co), squares (Ni), stars (Mg), double circles (Cu), and composite triangles (Zn) indicate a single-phase MSeO$_3$ or MTeO$_3$.

the tellurite $CoTeO_3$, Small, nearly spherical crystals ($50 \sim 100$ μm in diameter) were picked up from the run products quenched from above 950°C. Their precession or Weissenberg photographs showed the systematic absence of the reflections $hk0$ with $h = 2n + 1$ and $0kl$ with $k + l = 2n + 1$, which is consistent with a space group $Pn2_1a$ or $Pnma$.

The intensity measurements were made with a computer-controlled automatic RIGAKU four-circle diffractometer equipped with an Mo X-ray tube and a scintillation counter. All the possible reflections in one octant in the region $2\theta < 80°$ (100° in case of $MgSeO_3$) were recorded with the 2θ-ω scan method. The background was measured at the start and the end of each interval of integration. Those reflections for which the integrated intensity was not at least three times as large as background were regarded as unobserved. The numbers of observed reflections are given in the last row of Table II. The integrated intensities were then converted to structure factors by applying Lorentz and polarization corrections.

Structure Refinements

Least-squares refinements were carried out with a local version of a full-matrix least-squares program LINUS (*10*). The atomic scattering factors for neutral atoms and the parameters for the anomalous dispersion were taken from the "International Tables for X-ray Crystallography" (*11*). A weighting factor was taken as 1.0 for each reflection.

The centrosymmetric space group *Pnma* with a cell composed of a four-formula unit was assumed and atoms were placed in the following way:

M	in	4(b):	0,	0, $\frac{1}{2}$
A	in	4(c):	x,	$\frac{1}{4}$, z
O(1)	in	4(c):	x,	$\frac{1}{4}$, z
O(2)	in	8(d):	x,	y, z.

The starting positional parameters for $CoSeO_3$, which was at first analyzed, were those of $LuFeO_3$, reported by Marezio, Remeika, and Dernier (*12*). In other selenites, the final values of $CoSeO_3$ were used as the starting parameters. For $CuSeO_3$ and $CoTeO_3$ similar values were used, but the sign of the

TABLE II

FINAL ATOMIC COORDINATES AND R FACTOR

		$MgSeO_3$	$MnSeO_3$	$CoSeO_3$	$NiSeO_3$	$CuSeO_3$	$ZnSeO_3$	$CoTeO_3$
A	x	0.0234	0.0257	0.0229	0.0207	0.0407	0.0266	−0.0103
	z	−0.0178	−0.0172	−0.0170	−0.0189	0.0029	−0.0161	−0.0131
O (1)	x	0.0700	0.0798	0.0720	0.0722	0.0791	0.0793	0.0499
	z	0.3199	0.3089	0.3206	0.3234	0.3315	0.3184	0.3375
O (2)	x	0.1823	0.1794	0.1832	0.1831	0.2023	0.1838	0.1828
	y	0.0795	0.0836	0.0778	0.0754	0.0728	0.0785	0.0655
	z	0.8621	0.8673	0.8663	0.8599	0.9066	0.8660	0.8660
R		0.042	0.034	0.026	0.028	0.069	0.091	0.047
Number of observed reflections		704	603	470	465	631	472	658

TABLE III

FINAL THERMAL PARAMETERS ($\times 10^4$)

		$MgSeO_3$	$MnSeO_3$	$CoSeO_3$	$NiSeO_3$	$CuSeO_3$	$ZnSeO_3$	$CoTeO_3$
M	β_{11}[a]	48.1	48.1	41.8	36.0	43.6	69.1	19.4
	β_{22}	20.7	31.2	23.9	17.1	30.3	29.0	22.0
	β_{33}	48.5	63.1	61.2	41.2	53.6	102.2	48.3
	β_{12}	0.5	2.4	3.0	−0.1	9.0	5.1	0.2
	β_{23}	−4.4	−2.6	−5.9	−0.3	−25.7	−20.7	−7.5
	β_{31}	0.5	3.6	−0.9	−0.3	−14.0	−2.2	−5.3
A	β_{11}	28.2	34.4	28.9	24.7	37.6	42.2	13.9
	β_{22}	15.5	27.4	20.3	16.2	26.1	27.2	20.7
	β_{33}	27.1	40.2	49.0	29.7	29.1	70.7	31.1
	β_{13}	−1.2	−3.2	−2.6	−2.7	7.0	−1.9	0.9
O (1)	β_{11}	47.9	60.4	48.7	52.9	74.9	16.4	45.6
	β_{22}	18.8	39.2	32.6	12.8	43.6	26.3	6.9
	β_{33}	36.3	37.7	48.4	35.8	22.9	133.3	47.5
	β_{13}	3.7	−15.6	2.1	6.5	9.1	39.8	−14.1
O (2)	β_{11}	47.3	54.4	46.4	36.5	43.6	75.2	23.3
	β_{22}	23.4	33.8	24.6	20.1	29.6	28.6	24.3
	β_{33}	44.0	62.3	68.4	55.8	55.6	76.8	68.1
	β_{12}	1.8	14.9	11.4	9.4	10.3	19.6	2.5
	β_{23}	6.7	0.3	5.5	−4.0	10.1	−0.9	1.9
	β_{31}	−11.6	−16.7	−10.5	−12.6	6.0	−6.8	−24.9

[a] The anisotropic thermal parameters are the coefficients in the expression $\exp[-(\beta_{11}h^2 + \beta_{22}k^2 + \beta_{33}l^2 + 2\beta_{12}hk + 2\beta_{13}hl + 2\beta_{23}kl)]$.

parameter z of Se or x of Te was reversed. In the last several cycles, 29 parameters, the scale factor, the 7 positional parameters, the 20 thermal parameters, and the extinction parameter were varied. The R factors less than 0.091 were obtained in all the crystals analysed.

The final positional and thermal parameters are given in Tables II and III, respectively.

Magnetic Properties

Magnetic measurements of powder samples of $MnSeO_3$, $CoSeO_3$, $NiSeO_3$, $CuSeO_3$,

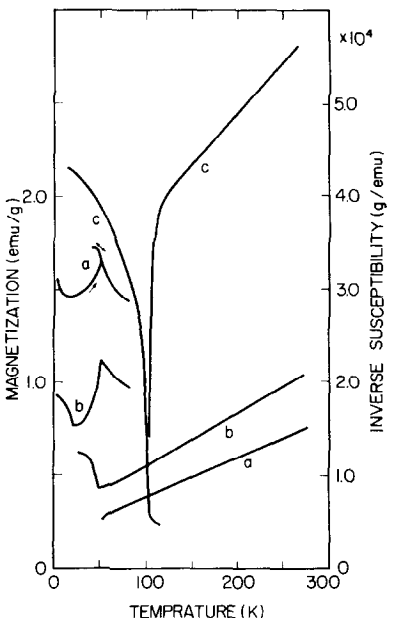

FIG. 2. Temperature dependence of the inverse susceptibility and the magnetization in the magnetic field of 9.59 kOe of $MnSeO_3$ (a), $CoSeO_3$ (b), and $NiSeO_3$ (c).

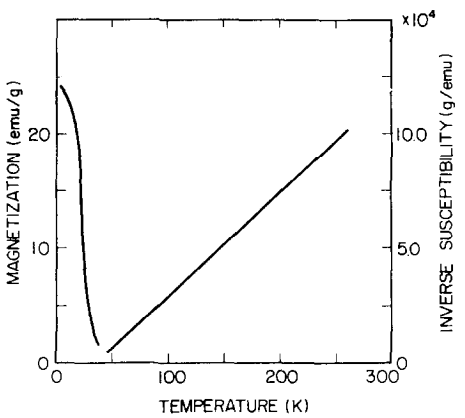

FIG. 3. Temperature dependence of the inverse susceptibility and the magnetization in the magnetic field of 9.59 kOe of $CuSeO_3$.

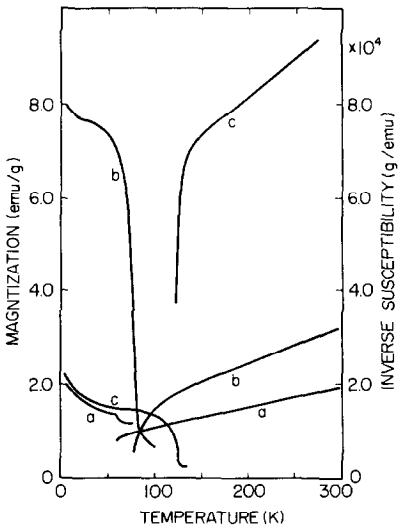

FIG. 4. Temperature dependence of the inverse susceptibility and the magnetization in the magnetic field of 9.59 kOe (10.0 kOe in case of $CoTeO_3$) of $MnTeO_3$ (a), $CoTeO_3$ (b), and $NiTeO_3$ (c).

$MnTeO_3$, $CoTeO_3$, and $NiTeO_3$ were made in the applied magnetic field up to 10 kOe. A vibrating sample magnetometer and a pendulum-type magnetometer were used. The results are given in Figs. 2, 3, and 4. The behaviors in higher temperature are well described by the Curie–Weiss law

$$\chi = \frac{N\mu_B{}^2 p_{\mathrm{eff}}^2}{3k} \cdot \frac{1}{T-\theta_p}$$

with the constants given in Table IV. The effective Bohr magneton number p_{eff} takes a typical value in Mn^{2+} and Co^{2+} compounds and $CuSeO_3$, but the values in Ni^{2+} compounds are somewhat higher than the usual one. All the compounds except $CuSeO_3$ become antiferromagnetic below a certain Néel temperature T_N given in the third row of Table IV. Weak ferromagnetism appears at T_N in these compounds except $CoSeO_3$. In $MnSeO_3$ and $CoTeO_3$, the saturation could not be attained in our measurements. Remarkable magnetic field annealing effect was observed in $MnSeO_3$: the magnetization during heating from 4.2°K in the magnetic field of 9.6 kOe is quite different from that after cooling from above T_N in the applied field.

TABLE IV

MAGNETIC PROPERTIES OF MAO_3

	$MnSeO_3$	$CoSeO_3$	$NiSeO_3$	$CuSeO_3$	$MnTeO_3$	$CoTeO_3$	$NiTeO_3$
p_{eff}	5.9	5.1	3.7	1.8	6.2	4.9	3.4
θ (°K)	−80	−90	−250	35	−130	−120	−270
T_N(°K)	51 ± 1	49 ± 1	98 ± 1	26 ± 2	61 ± 1	78 ± 2	125 ± 2

$CuSeO_3$ is a ferromagnet with the Curie temperature of 26°K. The magnetization at 4.2°K in the magnetic field of 9.6 kOe is 24.1 emu/g and still unsaturated. If all the Cu^{2+} moments give rise to magnetic ordering, the saturation magnetization at 0°K will be 29.3 emu/g.

Description of the Structure and Discussion

The interatomic distances and angles were calculated with the program DAPH or RSDA-4 (*13*). They are given in Tables V, VI, and VII. Figures 5 and 6 show the projections of the structure of $CoSeO_3$ and $CoTeO_3$ on the *ac* plane. The difference is found in the direction of the shift of Se or Te from the ideal position 0, ¼, 0. All the other selenites have a similar structure. Oxygen octahedra surrounding an *M* atom are outlined in the figures.

This structure can be described from two different standpoints. At first it is considered to be a salt of M^{2+} and AO_3^{2-} ions. They are situated at the points of a body-centred lattice alternatively. An AO_3^{2-} is a trigonal pyramid with three oxygens at the corners of basal triangle and an *A* atom at the fourth corner. Each M^{2+} is linked to three AO_3^{2-} ions. As observed from Table V, an SeO_3 group has almost the same shape and size in all the $MSeO_3$ compounds reported here. In VSe_2O_6 (*14*), $CuSeO_32H_2O$ (*15*), and $ZnSe_2O_5$ (*16*), the only selenites with the published structure data, similar SeO_3 groups with an average Se–O distance of 1.725, 1.757, or 1.727 Å, respectively, are observed. These evidences support the view that an SeO_3 group is an independent unit in the structure. A TeO_3 group in $CoTeO_3$ has a similar shape, but it is somewhat more flattened than SeO_3 groups and an average TeO_3 in other tellurites

TABLE V

INTERATOMIC DISTANCES (Å) AND ANGLES (°) BETWEEN AN *A* ATOM AND THE NEIGHBORING OXYGEN ATOMS

	$MgSeO_3$	$MnSeO_3$	$CoSeO_3$	$NiSeO_3$	$CuSeO_3$	$ZnSeO_3$	$CoTeO_3$
*A*ii–O(1)i	1.712	1.710	1.719	1.718	1.751	1.717	1.902
*A*ii–O(1)iv	2.863	2.921	2.844	2.809	2.889	2.841	2.807
*A*ii–O(1)iii	3.327	3.484	3.336	3.263	3.554	3.372	3.478
*A*ii–O(1)ii	3.386	3.544	3.395	3.383	3.329	3.433	3.498
*A*ii–O(2)ii (×2)	1.720	1.716	1.716	1.731	1.695	1.723	1.920
*A*ii–O(2)vi (×2)	2.914	3.007	2.869	2.837	2.815	2.916	2.704
*A*ii–O(2)iii (×2)	2.961	3.068	2.969	2.916	3.231	2.996	2.978
*A*ii–O(2)vii (×2)	3.610	3.746	3.591	3.539	3.104	3.607	3.149
Average *A*–O distance in AO_3 group	1.717	1.714	1.717	1.727	1.714	1.724	1.914
O(1)ii–*A*ii–O(2)v	104.9	103.5	104.0	104.1	104.9	104.1	102.4
O(2)v–*A*ii–O(2)vi	95.1	95.3	95.1	95.0	95.1	95.4	114.6

TABLE VI

INTERATOMIC DISTANCES (Å) AND ANGLES (°) IN MO_6 OCTAHEDRA

	$MgSeO_3$	$MnSeO_3$	$CoSeO_3$	$NiSeO_3$	$CuSeO_3$	$ZnSeO_3$	$CoTeO_3$	$LuFeO_3$
*M*ii–O(1)i	2.158	2.252	2.140	2.116	2.090	2.177	2.090	2.008
*M*ii–O(2)vi	2.196	2.281	2.214	2.154	2.521	2.223	2.292	2.024
*M*ii–O(2)vii	2.095	2.172	2.076	2.067	1.919	2.089	2.096	1.997
O(1)i–O(2)vii	2.929	3.021	2.885	2.845	2.729	2.897	2.869	2.793
O(1)i–O(2)vi	3.073	3.194	3.055	3.011	3.161	3.107	2.958	2.884
O(1)i–O(2)ii	3.085	3.216	3.104	3.029	3.385	3.116	3.239	2.779
O(1)i–O(2)iii	3.085	3.232	3.076	3.067	2.942	3.132	3.049	2.908
O(2)vi–O(2)vii	3.168	3.278	3.180	3.134	3.411	3.190	3.252	2.845
O(2)vi–O(2)iii	2.897	3.015	2.883	2.829	2.905	2.904	2.952	2.842
Average *M*–O distance	2.150	2.235	2.143	2.112	2.177	2.143	2.159	2.010
Average O–O distance	3.040	3.159	3.103	2.986	3.089	3.058	3.053	2.842
O(1)i–*M*ii–O(2)vii	87.0	86.1	86.3	85.7	85.7	85.5	86.5	87.7
O(1)i–*M*ii–O(2)iv	89.8	89.6	89.1	89.7	86.0	89.8	84.8	87.9
O(2)vii–*M*ii–O(2)vi	95.1	94.8	95.6	95.9	99.5	95.4	95.6	90.1

TABLE VII

ANGLES (°) SPECIFYING THE TILT OF MO_6 OCTAHEDRA

	$MgSeO_3$	$MnSeO_3$	$CoSeO_3$	$NiSeO_3$	$CuSeO_3$	$ZnSeO_3$	$CoTeO_3$	$LuFeO_3$
θ^a	14.2	15.2	14.4	14.1	15.0	14.6	13.5	10.1
ϕ^b	111.2	112.7	111.9	112.3	115.2	113.6	107.0	22.2
ψ^c	20.8	21.6	21.5	20.3	29.0	21.5	22.4	−12.9
*M*ii–O(1)i–*M*i	125.3	121.7	124.5	125.4	122.4	123.5	128.0	140.7
*M*ii–O(2)vii–*M*iii	129.3	127.6	129.4	130.9	127.1	129.4	132.5	142.4

[a] θ is the angle between the b-axis and the vector $\overrightarrow{M\text{ii}O(1)}$.

[b] ϕ is the azymuthal angle of the vector $\overrightarrow{M\text{ii}O(1)}$ measured from the a-axis.

[c] ψ is the angle between the a axis and the vector connecting *M*ii to the midpoint of O(2)ii and O(2)vi. Both ϕ and ψ are measured counter clockwise around the b-axis.

(*17*, *18*). The features of these AO_3 groups will be discussed later.

From another view, MAO_3 crystals have a distorted perovskite ABX_3 structure, in which A^{4+} ions occupy the larger A cation sites and M^{2+} the B sites. This structure is composed of BX_6 octahedra, which are linked together at the corners to form a three-dimensional network, and A cations in the cavities of this network. In an ideal perovskite, an A cation is surrounded by 12 anions X at an equal distance. In the selenites and tellurites reported in this paper, however, an A^{4+} ion with a relatively small size and strong covalent character attracts 3 out of 12 oxygens to the distance of contact, while the others are far apart and linked to other A^{4+} ions. Thus an AO_3 group rather than A^{4+} ion surrounded by 12 oxygens is a natural component of the structure. On the other hand, MO_6 octahedra are easily distinguished, as shown in Figs. 5 and 6. The displacement of oxygens toward

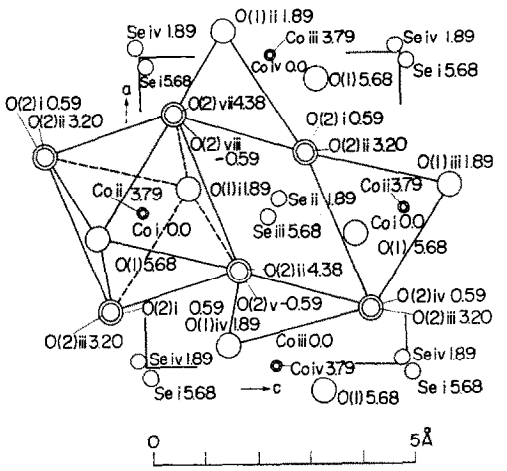

FIG. 5. The projection of a unit cell of $CoSeO_3$ on the *ac* plane. The heights of the atoms are in ångströms. An oxygen–metal octahedron is outlined.

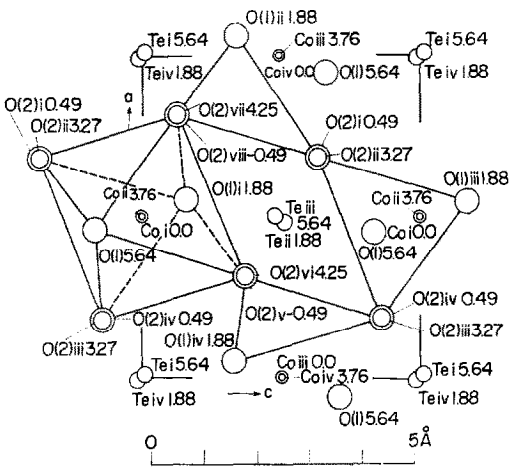

FIG. 6. The projection of a unit cell of $CoTeO_3$ on the *ac* plane. The heights of the atoms are in ångströms. An oxygen–metal octahedron is outlined.

an A^{4+}, however, cause an unusually large distortion and tilt of these octahedra,[1] which are specified by the interatomic distances and angles in Tables VI and VII. The tilt angles θ and ϕ of an octahedron are the polar and azymuthal angles of the vector combining M to O(1)i with respect to the unit cell edges. The angle ψ is the one between the *a*-axis and the vector combining M to the midpoint of O(2)ii and O(2)vii. The parameters of $LuFeO_3$, which are taken as a representative example of perovskite oxides with tilted octahedra, are listed for the sake of comparison. It is noticeable that the distortion in an octahedron itself is quite small in orthoferrites and many other orthorhombic perovskite oxides. In spite of a large distortion, the average M–O distances are well understood on the conception of ionic radii with the exception of $CuSeO_3$. This trend shown in Fig. 7, indicates that the origin of the distortion does not come from an M^{2+} ion itself, which tends to retain its octahedral surroundings. This is also seen in the fact that the average Se–O distance in the SeO_3 group of the $MSeO_3$ is almost independent of the radius of M^{2+}. A larger distortion of an octahedron is observed in $CuSeO_3$, in which three body diagonals of the octahedron differ from each other by about 20%. This is due to the preference of a Jahn–Teller Cu^{2+} ion for non-octahedral bonding. The distortions of the same order of magnitude also have been observed in $KCuF_3$ (*19*) and $CuTe_2O_5$ (*20*).

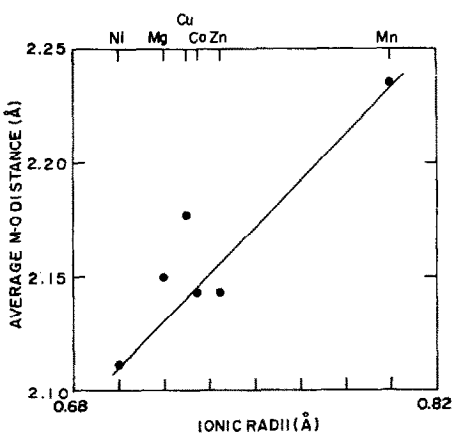

FIG. 7. The average M–O distance in MO_6 octahedra vs ionic radii of M^{2+} cations.

[1] The tilt of octahedra in perovskite structure is usually discussed in connection with the tolerance factor *t*. If we take the "ionic radii" of Se^{4+} and Te^{4+} as the difference between the average distance to the 12 neighboring oxygens and the radius of O^{2-}, we get the value of *t* nearly equal to 1.0. But such a discussion is not appropriate here, since ionic radius loses a definite meaning for Se^{4+} and Te^{4+} ions with a strong covalent character.

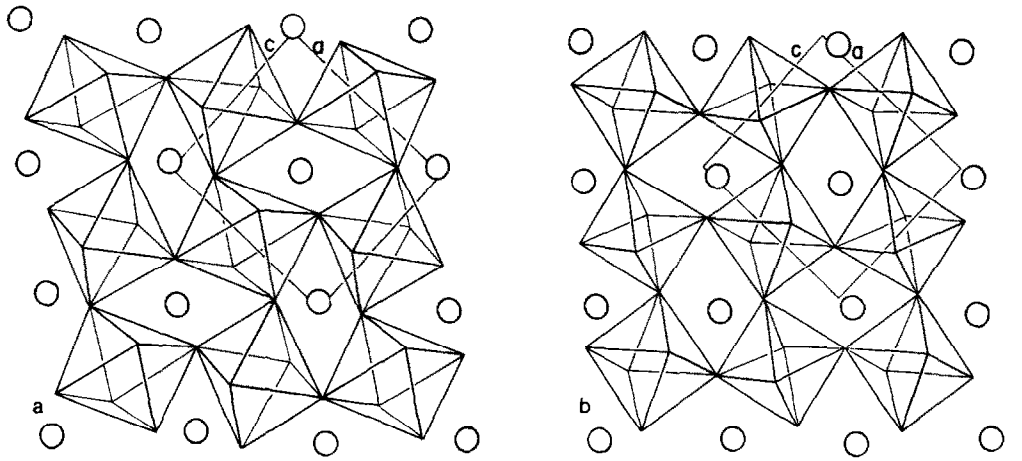

FIG. 8. Layer of octahedra in lower half of a unit cell projected on the *ac* plane. (a) $CoTeO_3$, (b) $LuFeO_3$. Open circles are A cations (Te or Lu, respectively) at height $\frac{1}{4}$.

The tilt of an octahedron is commonly observed in orthorhombic perovskites. A definite feature in the MAO_3 compounds reported here is that the sense of the tilt is opposite to that in usual cases. This is clearly seen from Fig. 8, in which a layer of octahedra in lower half of a unit cell is illustrated for $CoTeO_3$ and $LuFeO_3$. The sense of the tilt in the former is well understood by considering the shift of oxygens toward Te. Figures 5, 6, and 8 show that tilts repeat alternatively from one octahedron to the next and therefore the M–O–M angle deviates from 180°. In the MAO_3 compounds they take a value around 125°, which is much smaller than those in ordinary perovskite oxides.

As concluded from the above discussion, deviation of MSeO$_3$ and MTeO$_3$ from an ideal perovskite is anomalously large and can be attributed to the strong preference of Se^{4+} and Te^{4+} ions for unusual stereochemistry. In this sense these compounds are situated on the midway between a salt and a double oxide containing two kinds of metal ions.

The coordination of oxygen around an ion with a nonbonded *s*-electron pair has been widely discussed. The most common configuration is an AO_3 triangular pyramid or AO_4 distorted bisphenoid, which are illustrated in Fig. 9. They have been considered as an AO_6 octahedron, in which A is displaced along the threefold or twofold axis (*1*). In another interpretation (*3*) they are tetrahedral AO_3E or bipyramidal AO_4E molecule where a nonbonded pair E is directed toward an empty corner. They exist in crystals as a discrete unit or form a more complicated group like A_2O_5, A_2O_6, A_3O_8, etc., by having oxygens in common (*18*). The published structural data indicate that the A–O distances and the O–A–O angles take more scattered values, according as AO_3 or AO_4 units are grouped together in the higher degree. In other words, AO_3 or AO_4 units have more symmetric shape when they are isolated from each other. Since more dense structure requires more symmetric shape of its units, the structure with discrete AO_3 groups is expected for the high-pressure phase. In fact, the MAO_3 compounds reported in this paper have discrete AO_3 groups. On the other hand, most selenites and tellurites of divalent iron group

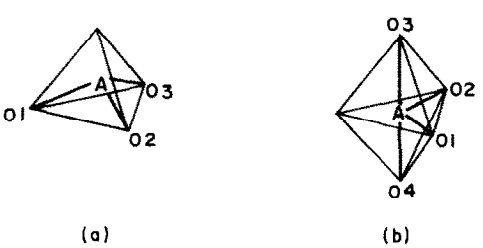

FIG. 9. Coordination of oxygen around Se or Te atoms. (a) Trigonal pyramid AO_3. (b) Distorted bisphenoid AO_4.

TABLE VIII

TRANSITION METAL SELENITES AND TELLURITES CONTAINING SeO_3 OR TeO_3 GROUPS

Substance	A_mO_n group		Interatomic distances[a] (Å)			Angles[a] (°)			Reference
			*A*O1	*A*O2	*A*O3	O2–*A*–O3	O3–*A*–O1	O1–*A*–O2	
VSe_2O_6	Se_2O_5	Se(1)	1.70	1.71	1.77	96.0	100.6	100.5	*14*
		Se(2)	1.70	1.66	1.82	100.6	96.3	103.4	
$CuSeO_3 \cdot 2H_2O$	SeO_3		1.72	1.77	1.72	98.5	96.0	98.5	*15*
$ZnSe_2O_5$	Se_2O_5		1.66	1.69	1.83	96.3	102.4	102.1	*16*
$\alpha TeVO_4$	TeO_3		1.81	1.95	1.99	94.0	98.5	92.0	*23*
$Co_6Te_5O_{16}$	TeO_3	Te(1)	1.86	1.87	1.88	92.5	98.2	103.3	*24*
		Te(2)	1.83	1.91	1.91	95.5	93.1	93.1	
		Te(3)	1.86	1.86	1.90	100.4	97.1	97.1	
$CuTeO_3 \cdot 2H_2O$	TeO_3		1.81	1.88	1.88	96.3	98.2	102.1	*25*
$CuTe_2O_5$	Te_2O_5	Te(1)	1.88	1.88	1.93	91.0	92.8	94.6	*20*
$CuTeO_3$	Te_2O_5	Te(2)	1.89	1.89	1.86	95.6	95.6	92.7	*28*
$ZnTeO_3$	TeO_3		1.86	1.87	1.90	98.1	95.0	95.4	*27*
$Zn_2Te_3O_8$	Te_3O_8	Te(2)	1.88	1.93	1.98	79.9	93.9	98.2	*7*

[a] The nomenclatures of distances and angles are shown in Fig 9(a).

TABLE IX

TRANSITION METAL SELENITES AND TELLURITIES CONTAINING SeO_4 OR TeO_4 GROUPS

Substance	A_mO_n group		Interatomic distances[a] (Å)				Angles[a] (°)		Reference
			*A*O1	*A*O2	*A*O3	*A*O4	O1–*A*–O2	O3–*A*–O4	
$TiTe_3O_8$	$(Te_3O_8)_\infty$ network		1.85	1.85	2.12	2.12	102.2	159.2	*26*
$\beta VTeO_3$	Te_2O_6		1.85	1.87	2.02	2.20	95	147	*29*
$Co_6Te_5O_{16}$	TeO_4	Te(4)	1.89	1.92	2.05	2.05	112.6	150.5	*24*
$CuTe_2O_5$	Te_2O_5	Te(1)	1.86	1.87	2.02	2.40	99.0	166.6	*20*
$CuTeO_3$	Te_2O_5	Te(2)	1.96	2.32	1.88	1.88	105.7	176.3	*28*
$Zn_2Te_3O_8$	Te_3O_8	Te(1)	1.83	1.83	2.10	2.10	106.3	175.0	*7*

[a] The nomenclatures of distances and angles are shown in Fig. 9(b).

ions contain more complicated Se_mO_n or Te_mO_n groups as listed in Tables VIII and IX. Such a tendency is also noticed in some silicates synthesized at atmospheric and high-pressure conditions. Some pyroxenes or pyroxenoids with SiO_4-chain transform to spinel plus stishovite (e.g., $MgSiO_3$, $FeSiO_3$, $CoSiO_3$) or to garnet (e.g., $MnSiO_3$) at high pressures (*21*). It is well known that SiO_4 groups are isolated in silicate spinel and garnet.

The ratio of metal to oxygen M/O in selenites and tellurites is larger when the Se_mO_n or Te_mO_n groups are more simple. Thus, we can expect to get the compounds with larger M/O ratio under high-pressure conditions. Since M ions often play an important role in determining physical properties of a crystal, we can conclude that high-pressure synthesis will be one of the useful tools in the crystal chemical research of new compounds

of the ions with nonbonded *s*-electron pair, such as selenites, tellurites, etc.

The paramagnetic Curie temperature and the Néel temperature of the MSeO$_3$ and MTeO$_3$ compounds reported in this paper generally decrease when we proceed from Mn to Ni along the row of the periodic table. This behavior is also observed widely in other magnetic oxides of iron group ions (*22*). The origin of ferromagnetic couplig in CuSeO$_3$ is not clear at present. As far as we know, this is the first example of ferromagnetic oxides containing no magnetic ions other than Cu^{2+}.

Acknowledgments

We are grateful to Professor Y. Saito, Professor N. Morimoto, Dr. I. Kawada, and Professor J. Kobayashi and the members of their research groups for affording us the facilities of using their X-ray apparatuses and kind assistances in operating them. We also express our sincere gratitude to Professor F. Marumo and Dr. M. Konno. We could not have completed the structure analyses without their valuable advice. We are grateful to Professor Y. Matsui, Professor Y. Syono, and Dr. Y. Uesu for discussions about the crystal structures. The assistance of K. Asai and H. Suwa are heartily acknowledged. This work has been partly supported by a Grant-in-Aid for Fundamental Research from the Japanese Ministry of Education.

References

1. L. E. ORGEL, *J. Chem. Soc.* 3815 (1959).
2. R. J. GILLESPIE, "Molecular Geometry," Van Nostrand, London (1972).
3. J. G. BERGMAN, JR., G. D. BOYD, A. ASHKIN, AND S. K. KURTZ, *J. Appl. Phys.* **40**, 2860 (1969).
4. For the review about these compounds, see G. A. SMOLENSKY *et al.*, "Ferroelectrics and Antiferroelectrics" (in Russian), Chap. 19, Izd. Nauka (1971).
5. K. KOHN, S. AKIMOTO, Y. UESU, AND K. ASAI, *J. Phys. Soc. Japan* **37**, 1169 (1974).
6. K. KOHN, S. AKIMOTO, K. INOUE, K. ASAI, AND O. HORIE, *J. Phys. Soc. Japan* **38**, 587 (1975).
7. K. HANKE, *Naturwissenschaften* **53**, 273 (1966).
8. M. TRÖMEL, D. SCHMID, AND ZIETHEN-REICHNACH, *Naturwissenschaften* **57**, 495 (1970).
9. G. PEREZ, F. LASSERRE, J. MORET, AND B. FRIT, *C. R. Acad. Sci. Paris* **272C**, 78 (1971)
10. P. COPPENS AND W. C. HAMILTON, *Acta Crystallogr.* **A26**, 71 (1970).
11. "International Tables for X-ray Crystallography," Vol. III, Kynoch Press, Birmingham (1962).
12. M. MAREZIO, J. P. REMEIKA, AND P. D. DERNIER, *Acta Crystallogr.* **B26**, 2008 (1970).
13. T. SAKURAI, "Universal Crystallographic Computation Program System (UNICS) I" (in Japanese), pp. 76, 78, The Crystal. Soc. Japan, Tokyo (1967).
14. G. MEUNIER, M. BERTAUD, AND J. GALY, *Acta Crystallogr.* **B30**, 2834 (1974).
15. V. GATTOW, *Acta Crystallogr.* **11**, 377 (1958).
16. G. MEUNIER AND M. BERTAUD, *Acta Crystallogr.* **B30**, 2840 (1974).
17. J. ZEMANN, *Monatshefte für Chemie* **102**, 1209 (1971).
18. I. D. BROWN, *J. Solid State Chem.* **11**, 214 (1974).
19. A. OKAZAKI AND Y. SUEMUNE, *J. Phys. Soc. Japan* **16**, 176 (1961).
20. K. HANKE, V. KUPCIK, AND O. LINDQVIST, *Acta Crystallogr.* **B29**, 963 (1973).
21. A. E. RINGWOOD, *Phys. Earth Planet. Interiors* **3**, 109 (1970).
22. K. MOTIDA AND S. MIYAHARA, *J. Phys. Soc. Japan* **28**, 1188 (1970).
23. G. MEUNIER, J. DARRIET, AND J. GALY, *J. Solid State Chem.* **5**, 314 (1972).
24. M. TRÖMEL AND TH. SCHELLER, *Naturwissenschaften* **57**, 495 (1970).
25. A. ZEMANN AND J. ZEMANN, *Acta Crystallogr.* **15**, 698 (1962).
26. G. MEUNIER AND J. GALY, *Acta Crystallogr.* **B27**, 602 (1971).
27. K. HANKE, *Naturwissenschaften* **54**, 199 (1967).
28. O. LINDQVIST, *Acta Chem. Scand.* **26**, 1423 (1972).
29. G. MEUNIER, J. DARRIET, AND J. GALY, *J. Solid State Chem.* **6**, 67 (1973).